Chapter 5

2D dynamical system

5.1 Introduction

In this chapter the dynamical system for the 2D driven cavity is discussed. In Section 5.2 the dynamical system is constructed, and models for the non-resolved modes are discussed. In Section 5.3 the short- and long-time integration of the dynamical system at Re=22,000 is discussed. The number of modes which is used ranges from 20 to 80. The dynamical behavior of the low-dimensional dynamical system is compared with the DNS. At Re=22,000, i.e. at the Reynolds number at which the POD is computed, the dynamical behavior of the dynamical system and DNS are similar both for short- and long-time integrations. Section 5.4 describes the behavior of the dynamical system at other Reynolds numbers. The transition analysis for the dynamical system is relatively cheap compared to the DNS. For the computation of instabilities of steady-state and periodic solutions we make use of linear stability analysis and Floquet multipliers (see Section 1.3).

It turns out that the transition from laminar to turbulent flow of the dynamical system is not exactly the same as the transition of the DNS which we have observed in Chapter 3. But we find solutions of the dynamical system which have the same dynamical behavior as solutions of the DNS.

5.2 Low-dimensional dynamical system

In section 2.4 the low-dimensional dynamical system has been derived by a Galerkin projection of the Navier-Stokes equations on the POD eigenfunctions. This system of ordinary differential equations for the coefficients a^k reads

$$\frac{\mathrm{d}a^k}{\mathrm{d}t} = -A_{kij}a^i a^j - B_{ki}a^i - C_k \tag{5.1}$$

a^k is the coefficient of the k^{th} POD eigenfunction in the expansion of the fluctuating velocity field $\mathbf{u}$. In (5.1) the terms A_{kij}, B_{ki}, and C_k are space-integrals of the POD eigenfunctions, the mean flow, and spatial derivatives of them (see (2.39)). The numerical space-integration is done by the trapezoidal integration rule, and for the convective and

dissipative terms the same second-order discretizations as in the DNS are used (see section 3.2).

For the time integration of equation (5.1) we have used different methods: 4^{th} order Runge-Kutta, trapezoidal rule with Newton linearization for the non-linear term, and 5^{th} order DOPRI with variable step size (see [24]). We have compared the methods and found that for accurate results we can use a larger time step for the dynamical system than for the DNS (for DNS 0.002 time units).

5.2.1 Closure models

We have used two different closure models for the non-resolved modes. These models have been described in Section 2.5. The first is the linear eddy-viscosity model defined by equation (2.39). The constant in this model has been determined by trial and error, such that the the energy distribution over the POD eigenfunctions is comparable to the eigenspectrum which follows from the DNS. It turns out that a value $1.2/N$ for the constant, where N is the number of POD eigenfunction, gives good results.

The second model is the linear damping model defined by equation (2.43). This model does not contain an adjustable constant, but it does depend on the number of POD eigenfunctions which are retained in the dynamical system. The amount of linear damping has been plotted in Fig. 5.1 in the form of a modified viscosity. This means that the term D_k in equation (2.43) has been incorporated in the term B_{kk} of equation (2.39) by means of a modification of the factor $1/Re$. In this way we have a reference for the order of magnitude of the damping coefficient. In Fig. 5.1 the first 21 modified coefficients are shown. We can see that some coefficients decrease compared to the simulation without a model, but on average they increase. It may be noted that in the 80-dimensional dynamical system the POD eigenfunction with index 46 has even a negative coefficient (not shown in Fig. 5.1). We can also see that the coefficients tend more to $1/Re$ if more POD eigenfunctions are retained in the dynamical system. This is what we expect because the more eigenfunctions are retained, the less eigenfunctions have to be modeled.

The main difference between the two models is that the linear damping model only modifies the $1/Re$ term of B_{kk}, and the linear eddy-viscosity model adjusts all the terms with a coefficient $1/Re$. We will see in the next sections that the linear damping model needs an additional modification. After that, it performs better than the linear eddy-viscosity model.

5.3 Dynamical system at Re=22,000

5.3.1 Short-time integrations

First we have performed short-time integrations to verify that the low-dimensional dynamical system converges to the DNS if we retain more POD eigenfunctions in the dynamical system.

The convergence of the solution of the 20, 40 and 80 dimensional dynamical systems to the solution of the DNS is shown in Fig. 5.2. Here, all integrations (i.e. of the Navier-Stokes equations and of the 20, 40 and 80 dimensional system) have been started

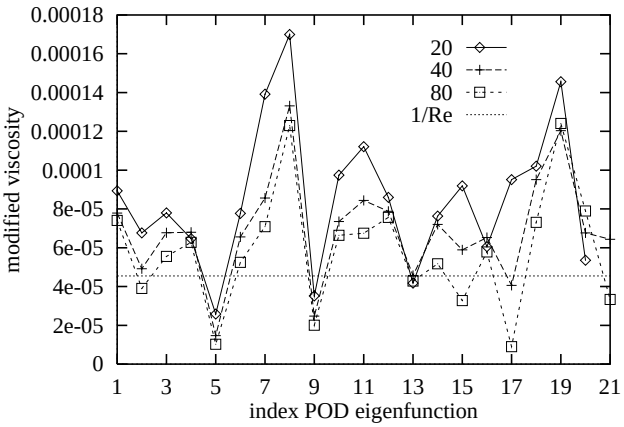

Figure 5.1: *The modified viscosity for the linear damping model as a function of the index of the POD eigenfunction. The modified viscosity is shown for no model (1/Re), the 20, the 40, and the 80 dimensional model.*

from identical initial conditions. The initial field is an arbitrary velocity field from the DNS time-series that has been projected on the first 20 eigenfunctions. For the 40 and 80 dimensional dynamical system the coefficients of the last 20 and the last 60 eigenfunctions have initially been set to zero respectively. We can see in Fig. 5.2 (left) that the dynamical system converges to the DNS if we take more POD eigenfunctions. In these plots the difference between the sum of the first 20 coefficients integrated in time of the DNS and the dynamical system is shown. The upper plot is without any model for the unresolved eigenfunctions, the middle plot with the linear eddy-viscosity model, and the lower with the linear damping model. We can see that from the top to the bottom the difference between dynamical system and DNS becomes a little smaller, but not significantly.

In Fig. 5.2 (right) the coefficients during 5 time units of the first POD eigenfunction are shown for the same models as in the left plots. It is clear that the 20-dimensional dynamical systems deviates the most from the DNS. The difference between the 40- and 80-dimensional dynamical system is less obvious.

5.3.2 Long-time integrations

The models for the non-resolved eigenfunctions in the dynamical system are based on the average energy content, they are incorporated to enable long-time integrations. Therefore the real comparison has to be made for long-time integration.

If we use no model, the 20-, 40-, and 80-dimensional dynamical system cannot be integrated over long times. It converges to a statistical equilibrium around non-physical solutions with a much to high energy content. So, obviously, we need a model.

The first model we have used is the linear eddy-viscosity model. We have integrated the dynamical system with this model for 1,750 time units. The results are shown in Fig. 5.3. We can see that the fluctuating energy has more peaks than the fluctuating energy of the DNS (see Fig. 3.10). For a fair comparison we should compare with the fluctuating energy contained in the first 80 POD eigenfunctions, but because they contain

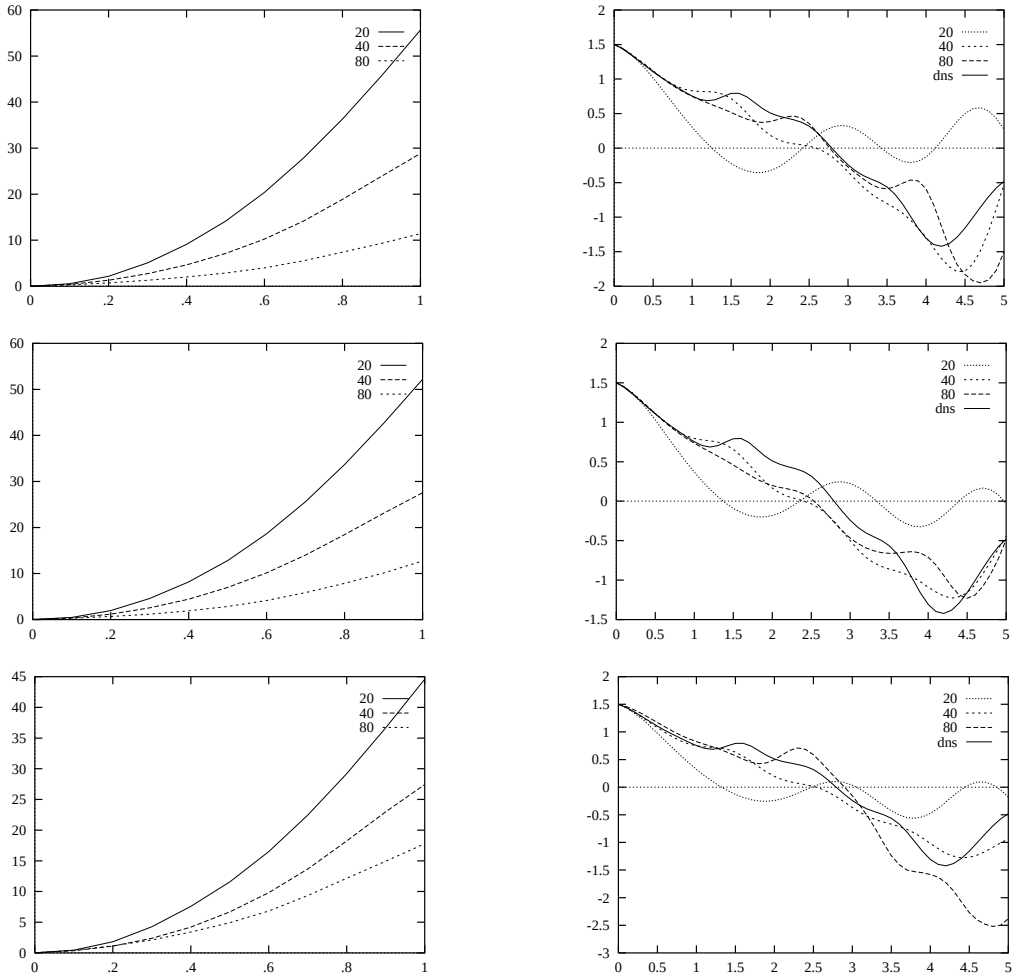

Figure 5.2: *The convergence of the low-dimensional dynamical system to the DNS as a function of the number of POD eigenfunctions. In each plot results of the dynamical system with 20, 40, and 80 POD eigenfunctions are shown. Left the sums of the deviations from the DNS of the first 20 coefficients integrated in time are shown. Right the coefficient of the coefficient of the first eigenfunction during the first 5 time units are shown. From top to bottom the dynamical system with no, the linear eddy-viscosity, and the linear damping model are used.*

approximately 95% of the fluctuating energy there is almost no difference. We can also see that the high peaks (over 0.01) present for the DNS are not present for the dynamical system.

The right-hand plot of Fig. 5.3 shows the spectrum (average energy per POD eigenfunction) of the dynamical system and the POD spectrum (POD eigenvalues) which follows from the DNS. We can see that too much energy is present in the direction of the eigenfunctions with a high index. Also the 17^{th} contains too much energy. The 17^{th} is the eigenfunction with the eddy in the core region of the cavity. This suggests that the dynamical system has a problem with the mechanism of building up the energy and then dissipating it by sending a vortex-structure into the core of the cavity.

It is clear that the dynamical system cannot accurately represent a vortex-structure moving in the core of the cavity due to the poor resolution of a vortex-structure in the

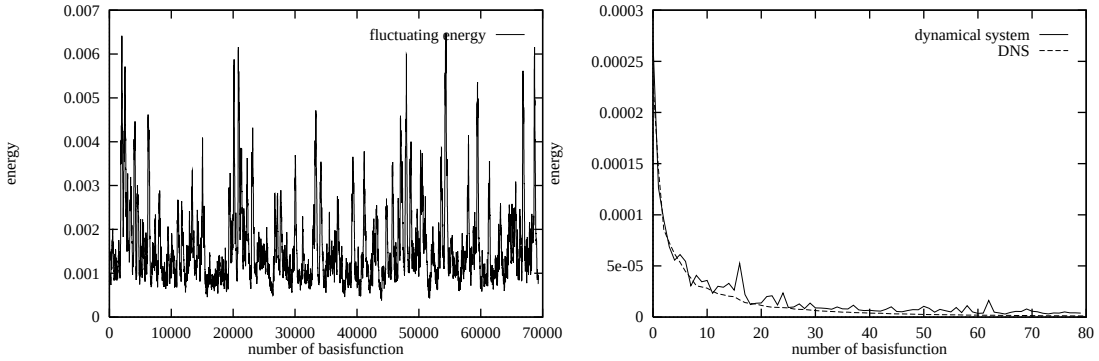

Figure 5.3: *Fluctuating energy and spectrum of the 80-dimensional dynamical system with the linear eddy-viscosity model.*

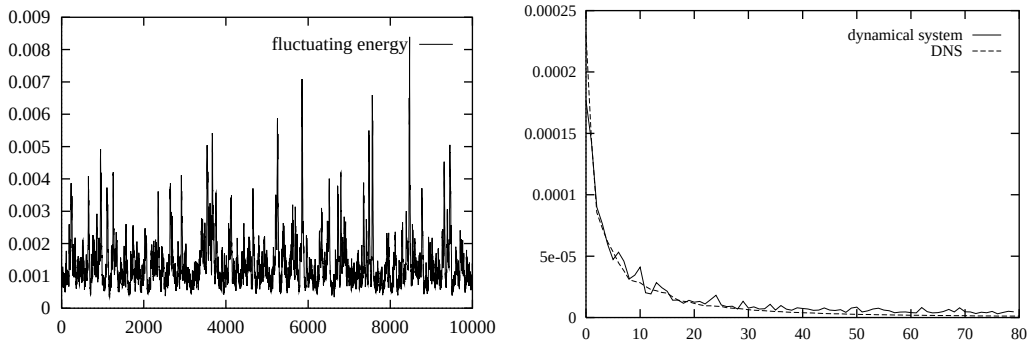

Figure 5.4: *Fluctuating energy and spectrum of the 80-dimensional dynamical system with the linear damping model.*

core in the snapshots used to compute the POD, since this happened only twice during the DNS which produced the snapshots (see Fig. 3.10). The high frequency of the peaks in the fluctuating energy can not be explained by this argument.

The second model that has been used for the long-time integrations is the linear damping model. As we have already mentioned in the previous section, some equations in the dynamical system get a negative damping. We have tried to integrate the model for a long time, but the dynamical system converged to a non-physical area of the state-space with a much too high energy level. Therefore, we set all the negative damping coefficients to zero, which means that all values below $1/Re$ in Fig. 5.1 are set at $1/Re$. After that modification the dynamical system has a physical solution. The results are shown in Fig. 5.4.

We can see in the left plot of Fig. 5.4 that we still find the frequent peaks in the fluctuating energy as with the linear eddy-viscosity model. The high peaks are also too low. This can be explained by the same argument as before: the dynamical system cannot represent a moving vortex-structure in the core region of the cavity.

The spectrum in the right-hand plot shows that the dynamical system does not have too much energy in the direction of the 17^{th} POD eigenfunction. This is an improvement compared to the linear eddy-viscosity model. The energy in the tail of the spectrum, however, is still too high.

5.4 Transition

In this section we perform a transition analysis with the low-dimensional dynamical system (see also [12]). A straightforward way to determine a solution at a certain Reynolds number is to integrate the dynamical system in time. For steady-state solutions a linear stability analysis can be performed, and a Floquet analysis can be performed for periodic solutions (see Section 1.3).

We do not use a model for the non-resolved eigenfunctions in the transition analysis because steady-state and periodic solutions are not turbulent and the models we have used were based on the energy cascade for turbulent flows.

We will use the 80-dimensional dynamical system for the transition analysis, unless stated otherwise.

5.4.1 Linear stability analysis

If we lower the Reynolds number for the dynamical system to Re=5,000, or lower, and integrate the system in time its solution converges rapidly to a steady-state. This happened for all initial values we tried. To determine the stability of these steady-state solutions we have linearized the low-dimensional dynamical system around the steady-state solution and computed the eigenvalues of the Jacobian (see equation (1.1)). The eigenvalues of the Jacobian for Re=5,000 are shown in Fig. 5.5. All eigenvalues have negative real parts indicating that small disturbances of the steady-state solution are damped.

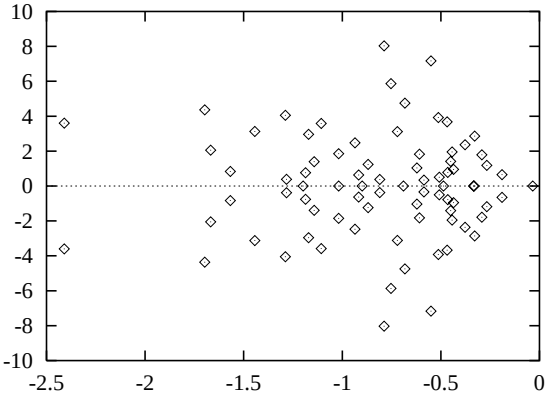

Figure 5.5: *Eigenvalues of the Jacobian of the linearized system at Re=5,000 in the complex plane. All eigenvalues have a negative real part indicating that the steady-state solution is stable.*

If we increase the Reynolds number the eigenvalues move towards the imaginary axis. To determine the bifurcation point where one or more eigenvalues cross the imaginary

axis we have computed the Jacobian at two different Reynolds numbers and extrapolated the smallest negative real part of the eigenvalues to zero assuming that the dependence on the Reynolds number is linear. By repeating this we have iterated to the bifurcation point. We found that at Re=7,819 a pair of complex conjugate eigenvalues crosses the imaginary axis indicating a Hopf bifurcation (see Fig. 5.6). The value Re=7,819 is close to the approximated first bifurcation Reynolds number of the DNS: 7,972 (see Chapter 3).

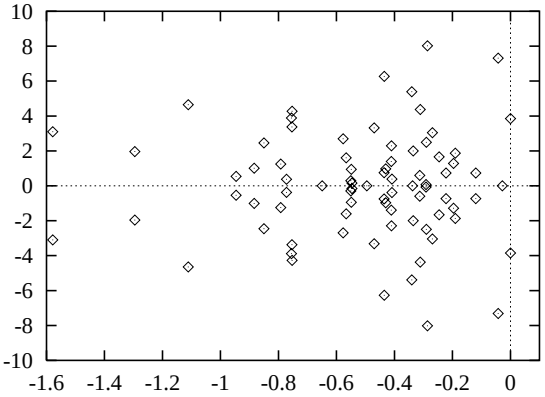

Figure 5.6: *Eigenvalues of the Jacobian of the linearized system at Re=7,819. A pair of complex conjugate eigenvalues crosses the imaginary axis.*

The period of the solution of the DNS at Re=8,000 is 2.2 time units. This is different from the period of the solution of the dynamical system just after the first bifurcation which is 1.63 time units. This is possibly caused by the mean flow at Re=22,000 which is a strong driving force in the dynamical system (see equation (1.3)). The flow at lower Reynolds numbers has a large amount of energy in the large eddy in the core of the cavity, whereas the mean flow at Re=22,000 has a relatively large amount of energy in the corners of the cavity. This means that the average velocity in the corners for the dynamical system is higher than for the DNS. Because the periodic solutions have their dynamics in the corners of the cavity we can expect a shorter period for the dynamical system.

To investigate the influence of the number of POD eigenfunctions retained in the dynamical system on the first bifurcation we have computed the first bifurcation Reynolds number for 20 to 80 eigenfunctions. The results are shown in Fig. 5.7. We can see large fluctuations till approximately 60 eigenfunctions. From 60 to 80 eigenfunctions the fluctuations are relatively low. But from 79 to 80 eigenfunctions the first bifurcation Reynolds number changes with more than 1,000. So, the small difference in the first bifurcation Reynolds number between the DNS and the 80-dimensional dynamical system is not stable to lowering the number of POD eigenfunctions. From Fig. 5.7 it seems that the dynamical system converges to a lower value for the first bifurcation Re-value than the value which follows from the DNS.

The eigenvector that corresponds to the unstable pair of complex conjugate eigenvalues shows which disturbances will grow in time for the dynamical system. The unstable eigenvector is shown in Fig. 5.8. The left plot shows the streaklines of the unstable

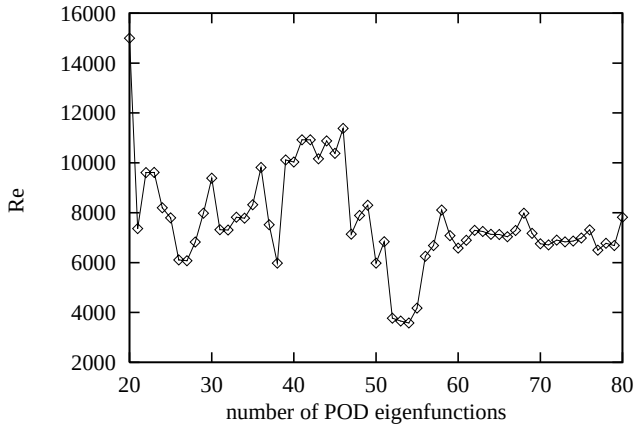

Figure 5.7: *Plot of the Reynolds number at which the first (Hopf) bifurcation takes place as a function of the number of POD eigenfunctions.*

eigenvector. We can clearly see some kind of vortex-street developing along the edge of the eddy in the core of the cavity. In the two right-hand plots we can see that the largest velocities are in the lower-right corner of the cavity, where the shear stress is largest. This indicates a shear layer instability.

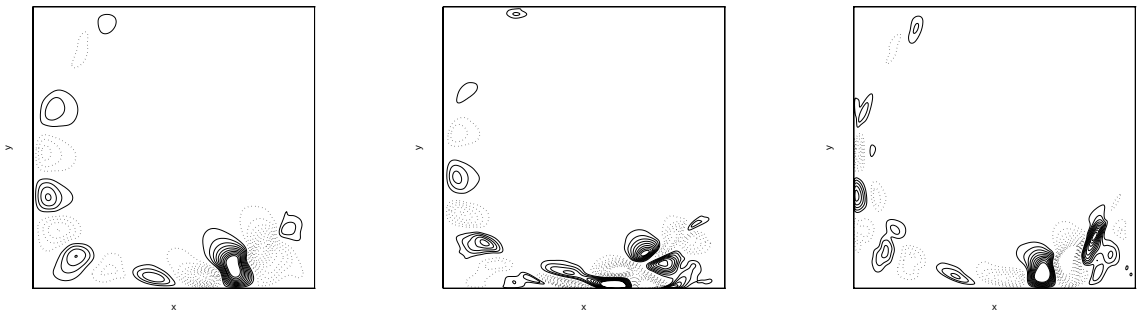

Figure 5.8: *The unstable eigenvector of the dynamical system at Re=7,819. From left to right is shown: streaklines, u-velocity ,and v-velocity. The solid lines indicates a positive value and the dotted lines a negative value.*

If we further increase the Reynolds number a second pair of eigenvalues crosses the imaginary axis, as shown in Fig. 5.9 (the top picture). The absolute imaginary part of these eigenvalues can be related directly to the period associated with the periodic solution; $P = 2\pi/\omega$ where P is the period, and ω is the absolute imaginary part of these eigenvalues. This means that this second pair of eigenvalues introduces a second period which is smaller than the period belonging to the first instability.

The eigenvector associated with this second instability is shown in the right (top) plot of Fig. 5.9. This eigenvector also shows a vortex street along the large eddy in the core of the cavity. It may be noted that the size of the eddies is smaller than in Fig. 5.8, i.e. the frequency of the solution is higher.

Further increasing the Reynolds number leads to a third, fourth, and fifth pair of eigenvalues crossing the imaginary axis. These are also shown in Fig. 5.9. It may be remarked that the second pair returns to the complex left half-plane before the fourth pair crosses the imaginary axis. We will see that something similar happens with the Floquet multipliers. When we look at the corresponding eigenvectors we see a vortex street for each eigenvector. There is a clear correspondence between the size of the eddies and the imaginary part of the eigenvalues crossing the imaginary axis. The largest velocity fluctuations appear in the lower-right corner for all but the fifth instability, this eigenvector has the largest fluctuations in the lower left side of the cavity.

We have to realize that after the first Hopf bifurcation the steady-state solution is unstable. So, the stability of the steady-state solution after the first bifurcation does not seem to be very interesting. The non-steady stable solution is determined by the non-linear terms which are neglected in the linear stability analysis. However, the amplitude of the periodic solutions is not very large and the mean flow is a strong driving force in the dynamical system. Consequently the instabilities of the steady-state solution are closely related to the instabilities of the non-steady solutions.

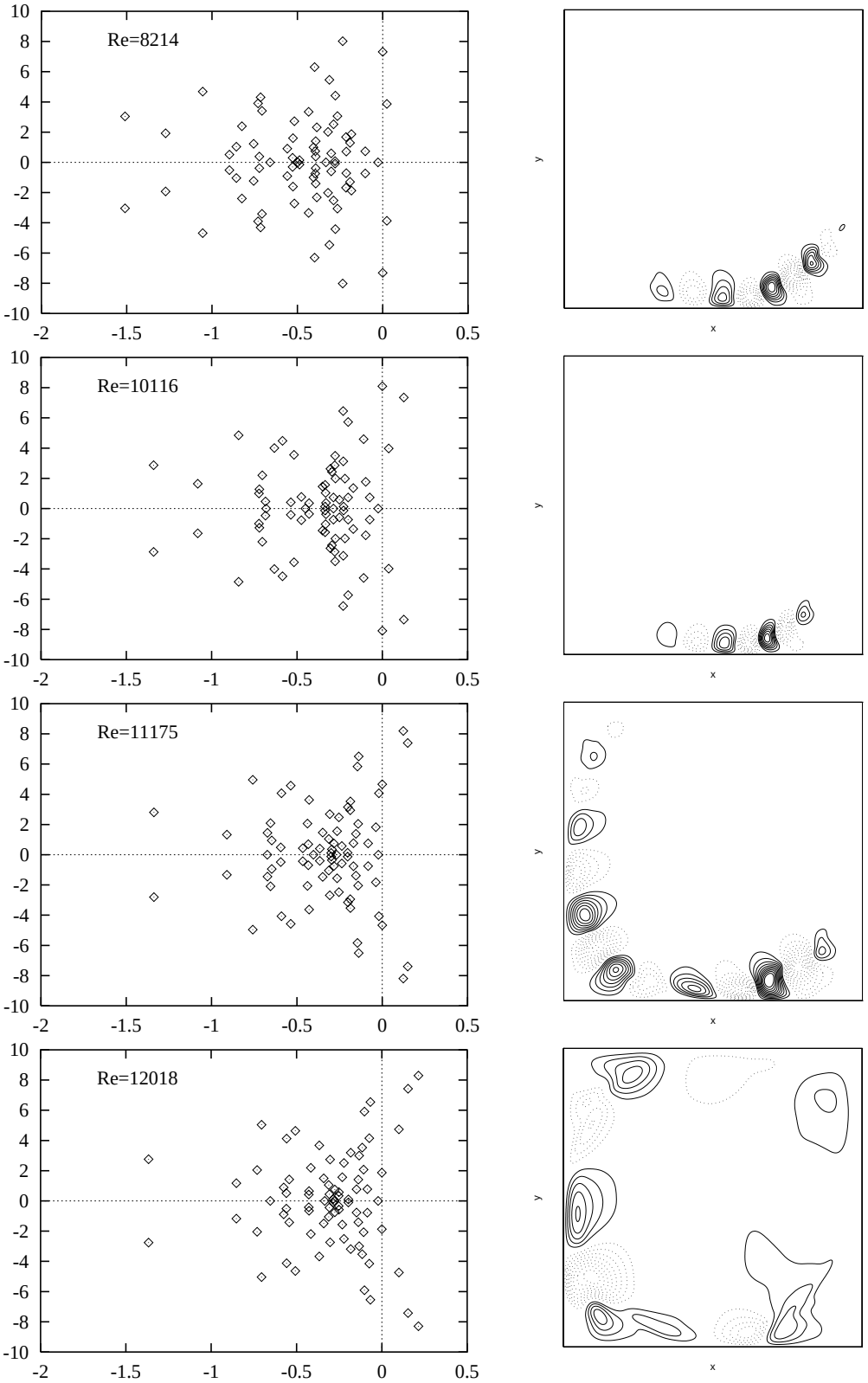

Figure 5.9: *Subsequent instabilities of the (unstable) steady-state solutions. Eigenvalues of the Jacobian (left) and streaklines (right) of the eigenvector belonging to the eigenvalue at the imaginary axis. The solid lines indicates a clock-wise turning direction and the dotted lines indicate a counter clock-wise turning direction.*

5.4.2 Floquet multipliers

A time-integration yields the periodic solution that appears after the first (Hopf) bifurcation, if the periodic solution is stable. The stability of a periodic solution is determined by its Floquet multipliers (see Section 1.3). A periodic solution is stable if all Floquet multipliers lie in the unit disc in the complex plane. If the periodic solution is not stable we cannot compute it by integrating the equations in time, sometimes reverse time-integration can be applied.

The numerical computation of the periodic solutions is done with the so-called *shooting method* (see [29]). The method starts with a solution in state-space $\boldsymbol{a}_s(\boldsymbol{x}, 0)$ sufficiently close to the periodic orbit. This initial solution has been determined by either a time-integration (for stable periodic solutions) or is taken equal to a solution which has been previously determined at a slightly different Reynolds number. Also a reasonable estimate of the period T_s of the periodic solution is needed.

From this starting solution we integrate the dynamical system over T_s time units. If we have not determined the periodic solution sufficiently accurate the difference between $\boldsymbol{a}_s(\boldsymbol{x}, T)$ and $\boldsymbol{a}_s(\boldsymbol{x}, 0)$ will not be zero. To find a solution which is accurate enough we have to solve the equation

$$\boldsymbol{a}_s(\boldsymbol{x}, T) - \boldsymbol{a}_s(\boldsymbol{x}, 0) = \mathbf{0}. \tag{5.2}$$

This equation is solved by the Newton method. The number of unknowns in this equation is $N + 1$, the number of coefficients N (=80) of the POD eigenfunctions plus the period T. We have only N equations for these unknowns. Therefore, one of the unknowns has to be fixed. We have to ensure that the value for this unknown lies on the periodic solution, if not we have to change it.

The Jacobian of equation (5.2) is equal to the matrix DP of equation (1.3) with an extra row and column for the partial derivatives with respect to T, and without the row and column corresponding to the fixed variable. For the numerical computation of this Jacobian we have not used equation (1.3), but we have integrated the modified Jacobian $\mathbf{J}$ numerically by applying equation (1.2) along the trajectory $\boldsymbol{a}_s(\boldsymbol{x}, t)$. We have used a 4^{th} order Runge-Kutta integration method for the integration of both the dynamical system and the modified Jacobian.

We have computed the periodic solution at Re=8,000. This solution is shown in Fig. 5.10. We can see that the most pronounced oscillations take place in the lower-right corner of the cavity. In the upper and lower left-corner we see almost no variations in the velocities. This could be expected because the unstable eigenvector has the largest variations in the lower-right corner.

For the computation of the Floquet multipliers we have used the same Jacobian as was used for the *shooting method* (without the partial derivatives with respect to the period T, and with the row and column corresponding to the fixed variable). We have computed the Floquet multipliers of the periodic solution at Re=8,000 which are shown in Fig. 5.11. This solution is stable since all the Floquet multipliers lie in the unit disc in the complex plane. It may be emphasized that the multiplier +1 is always present due to the fact that the right-hand side of equation (5.1) does not explicitly depend on the time t.

If we increase the Reynolds number to approximately Re=8,200, a pair of complex

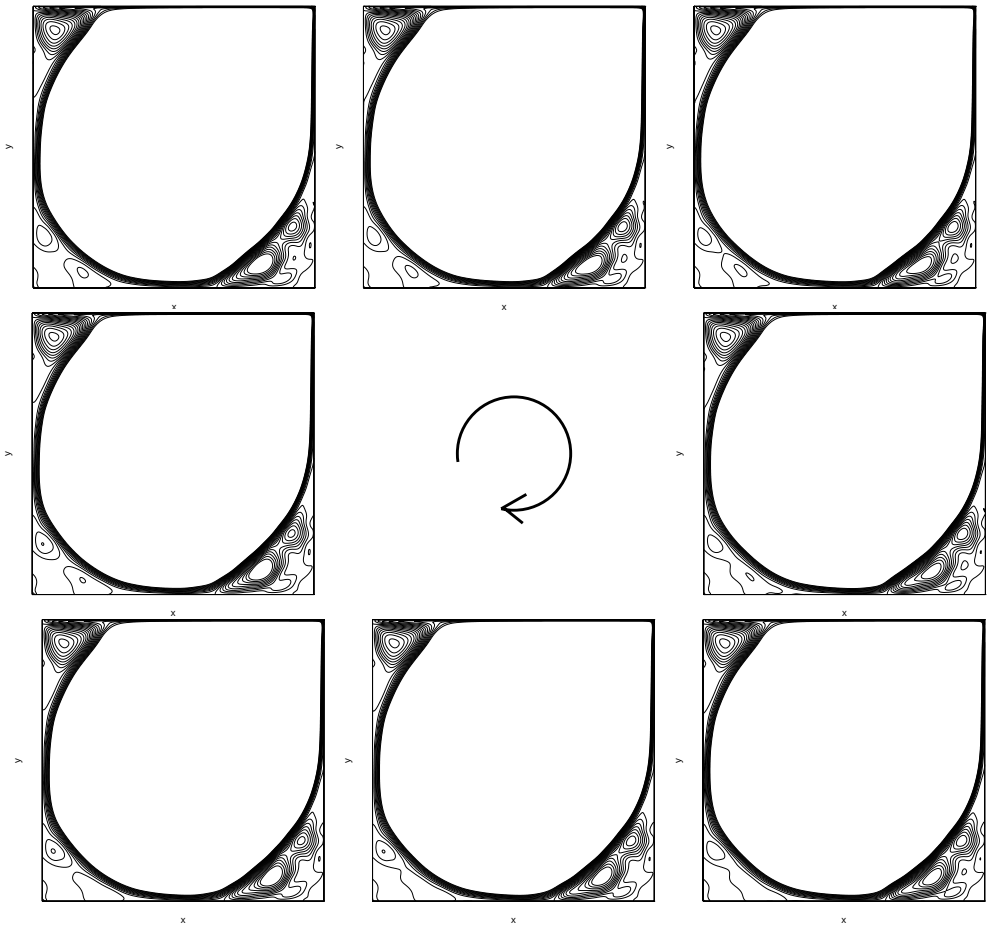

Figure 5.10: *One full period of streaklines of the periodic solution of the 80-dimensional dynamical system at Re=8,000. Both positive and negative turning-directions are solid lines.*

conjugate Floquet multipliers leave the unit disc, as is shown in Fig. 5.12. The two periods in this solution are 1.63 and 0.86 time units. This corresponds to the arguments of the pair of complex conjugate Floquet multipliers which leaves the unit disc. Indeed, the solution oscillates 1.63/0.86=1.9 times around the periodic solution with period 1.63, and the argument of the lower unstable Floquet multiplier is 1.9 times 2π.

This is also approximately the ratio between the imaginary parts of the first two pairs of unstable eigenvalues of the Jacobian of the steady-state solution (see Fig. 5.9). Thus, the amplitude of the oscillations the Floquet analysis and the linear analysis give similar results.

The unstable periodic solution stays unstable if we increase the Reynolds number. A second pair of Floquet multipliers leaves the unit disc at approximately Re=10,350. At Re=10,700 a Floquet multiplier leaves the unit disc at -1 indicating a period-doubling. These solutions are unstable with more than one period, and thus we can not compute them with our method. A time-integration starting from arbitrary conditions converged to the branch of periodic solutions for all starting conditions that we have tried. So we where not able to follow these other branches.

The stable 2-periodic solution that appears after the bifurcation at approximately

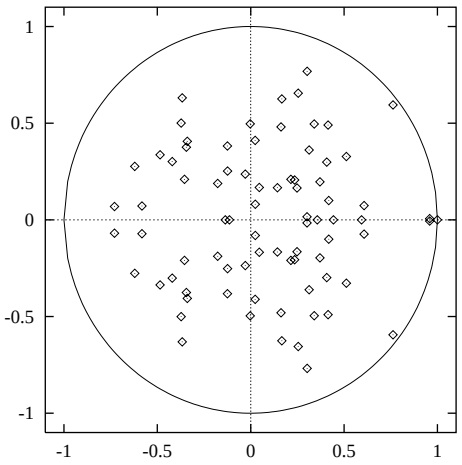

Figure 5.11: *Floquet multipliers of the the periodic solution at Re= 8,000. The solution is stable because all multipliers lie in the unit disc.*

Re=8,200 becomes 1-periodic again at approximately Re=8,400. The period of the solution is the period which belongs to the second pair of eigenvalues of the Jacobian which become unstable as is shown in Fig. 5.9. In Fig. 5.13 the Floquet multipliers which enter the unit disc are shown. This corresponds to an unstable periodic solution that becomes stable.

This solution with a period of 0.86 time units stays stable till approximately Re=8,750. Then a Floquet multiplier leaves the unit disc at -1, indicating a period-doubling (see Fig. 5.14). We have followed the periodic solution with the short period until Re=9,200. The unstable Floquet multiplier has then a relatively large absolute value and all other Floquet multipliers have an absolute value considerably smaller than one. So, the periodic solution is very unstable and converges rapidly to the stable periodic solution. We did not follow this branch further.

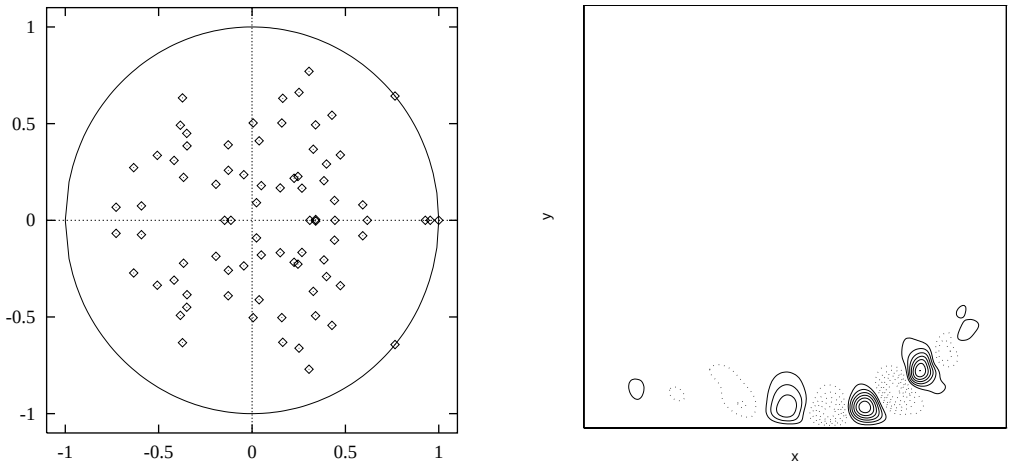

Figure 5.12: *Floquet multipliers of the the periodic solution at Re= 8,200. A pair of complex conjugate multipliers leaves the unit disc indicating that the periodic solution becomes unstable.*

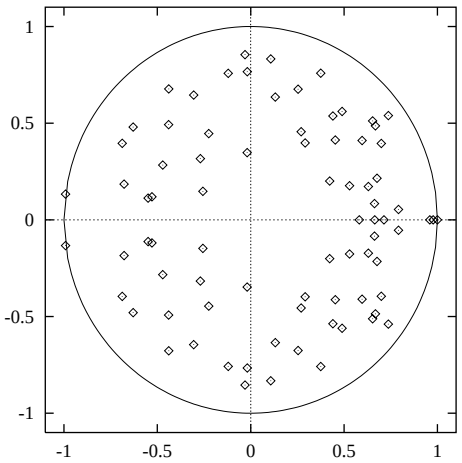

Figure 5.13: *Floquet multipliers of the the periodic solution at Re= 8,450. A pair of complex conjugate multipliers enters the unit disc indicating that the 2-periodic solution becomes stable.*

The periodic solution after the period-doubling remains stable for Reynolds numbers up to Re=11,188. Then a pair of complex conjugate Floquet multipliers leaves the unit disc as is shown in Fig. 5.15. The two periods of the 2-periodic solution are 1.67 and 2.70 time units. The unstable eigenvector belonging to the second period is also shown in Fig. 5.15. We can see a kind of vortex street developing like in Fig. 5.9. Here, however, the largest fluctuations are present in the lower-left corner of the cavity and not in the lower-right corner.

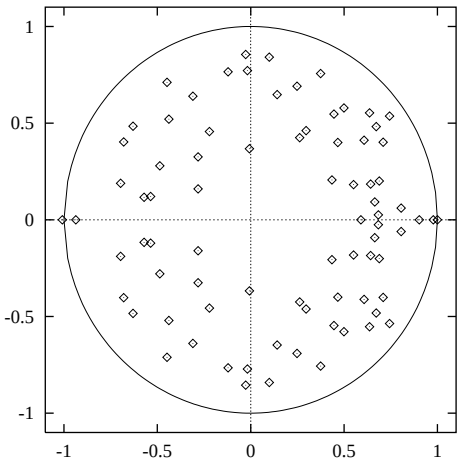

Figure 5.14: *Floquet multipliers of the the periodic solution at Re= 8,750. A real multiplier leaves the unit disc at -1 indicating that the periodic solution becomes unstable and undergoes a period-doubling.*

If we further increase the Reynolds number a pair of complex conjugate eigenvalues re-enters the unit disc at approximately Re=11,500. In Fig. 5.16 the Floquet multipliers for Re=11,000 to Re=13,000 are shown with steps of 100. We can see that the Floquet multiplier denoted by A first leaves the unit disc, and after that re-enters the unit disc.

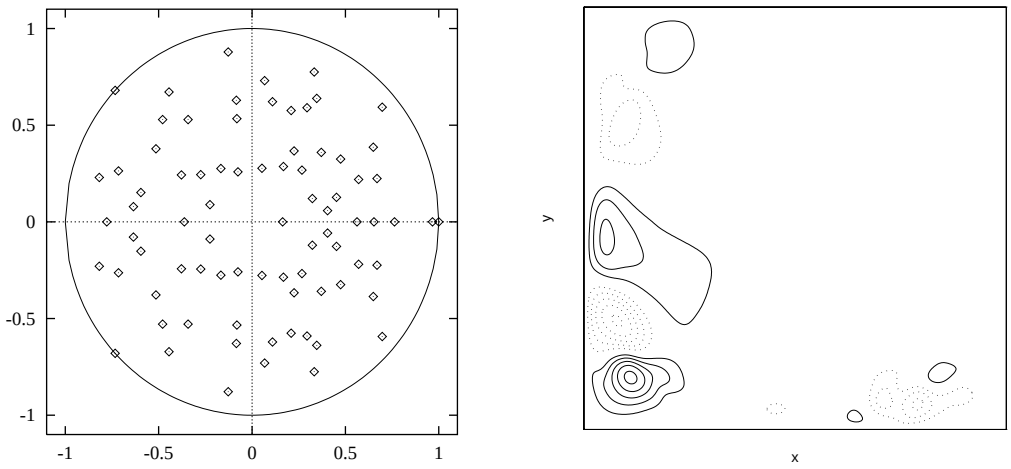

Figure 5.15: *Floquet multipliers (left) of the the periodic solution at Re= 11,118. A pair of complex conjugate multipliers crosses the unit disc indicating that the periodic solution becomes unstable. In the right-hand plot the eigenvector corresponding to the unstable Floquet multiplier is shown.*

The Floquet multiplier denoted by B moves to A. Then it is not clear whether A or B moves out of the unit disc. The eigenvector belonging to the Floquet multiplier which leaves the unit disc at approximately Re=11,900 is shown in Fig. 5.16. This eigenvector looks like the one belonging A (see in Fig. 5.15). The sign of the eigenvector has changed, but that isn't important.

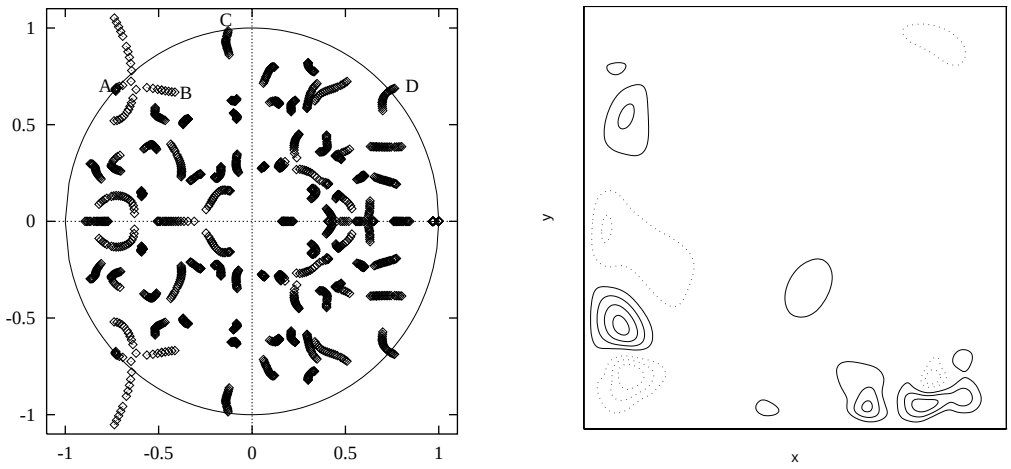

Figure 5.16: *Floquet multipliers (left) of the the periodic solutions from Re=11,000 to Re=13,000 with steps of 100. A pair of complex conjugate multipliers leaves the unit disc, re-enters, and again leaves the unit disc. In the right-hand plot the eigenvector corresponding to the unstable Floquet multiplier at Re=11,900 is shown.*

The (stable) periodic solution at Re=11,800 is shown in Fig. 5.17. Eddies in the lower-left corner of the cavity are aligned with the large eddy in the core of the cavity, and sometimes separated by flow entering from the core region in the lower-left corner. In the lower-right corner two eddies merge, and in between the merging flow from the core

enters.

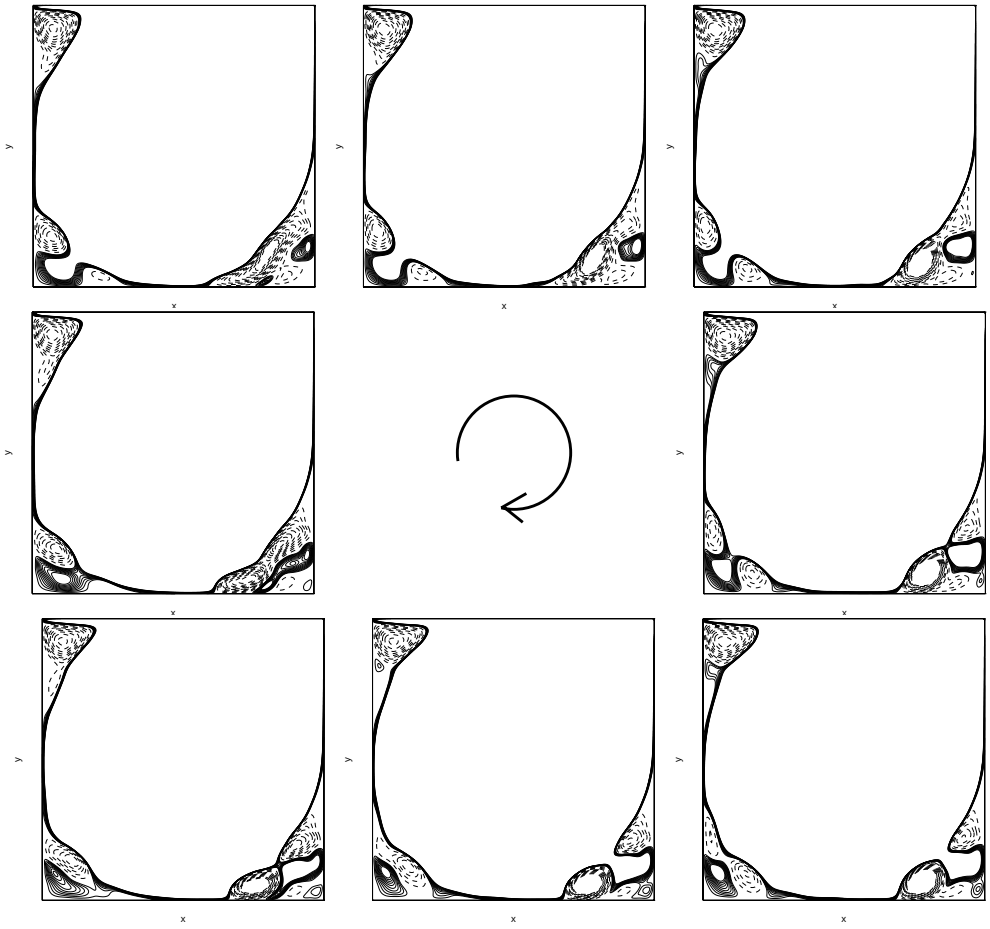

Figure 5.17: *Streaklines of one period of the periodic solution at* $Re = 11,800$. *Solid lines indicate a clock-wise rotation, and dashed lines indicate counter clock-wise rotation.*

5.4.3 Bifurcation diagram and comparison with DNS

In Fig. 5.18 the qualitative bifurcation diagram is shown. It is to be emphasized that the horizontal axis has a deformed scale. Moreover not all bifurcations from the steady-state solutions are shown for simplicity. In addition some branches could not be followed, so more solutions are possible. We can see that the periodic solution between Re=8,750 and Re=11,118 exists for a long range. The period of this solution is approximately the same as the period of the solution after the first Hopf bifurcation.

The behavior of the dynamical system in the range Re=8,200 and Re=8,750 is not found in the DNS computations of Chapter 3. It is possible that this does not 'really' happen, it is also possible that it is 'real' but that we did not find it.

The bifurcation of the dynamical system at Re=11,188 introduces two periods of which the ratio 2.70/1.67=1.6 is comparable to the ratio of the two periods of the 2-periodic solution of the DNS at Re=11,000: 3.70/2.33=1.6.

For higher Reynolds numbers both the DNS and the dynamical system have again periodic solutions. The period of the solutions of the dynamical system for Reynolds

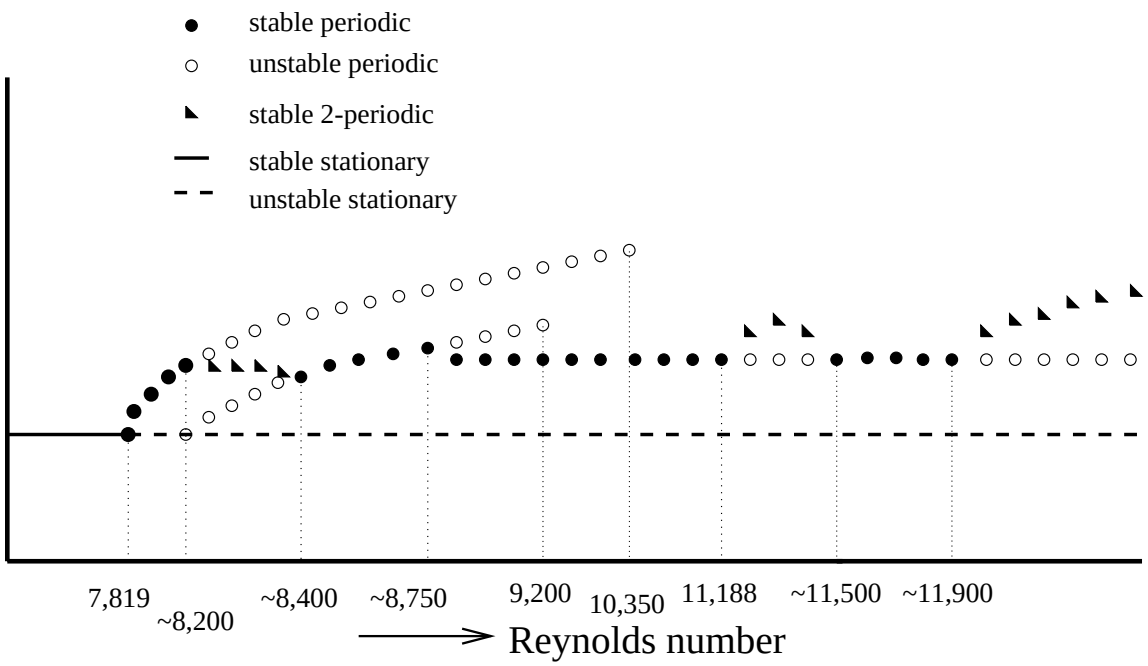

Figure 5.18: *Qualitative bifurcation diagram of the dynamical system. Not all the bifurcations from the steady-state solution are shown for simplicity. Note that the horizontal axis is not linear.*

numbers in the range Re=11,500-11,900 (i.e. 1.68) is almost the same as the period (1.69) of a periodic solution of the DNS at Re=12,000. The solutions shown in Fig. 5.10 and Fig. 3.8 show qualitatively the same behavior.

5.5 Conclusions

In this chapter we used the low-dimensional dynamical system to mimic DNS of the flow in a 2D driven cavity. We have described the models that we have used, did short- and long-time integrations at Re=22,000 (the Reynolds number at which the POD eigenfunctions are computed), and did a transition analysis. The results lead to the following conclusions.

- The low-dimensional dynamical system converges to the DNS when more POD eigenfunctions are retained in the dynamical system.
- We need a closure model for the non-retained POD eigenfunctions in the dynamical system to be able to integrate the dynamical system for long times.
- The modified linear damping model performed better than the linear eddy-viscosity model. Both had too low and too many peaks in the fluctuating energy compared to the DNS. This is partly due to the fact that the set of snapshots has a low resolution of eddies dissipating in the core of the cavity. If the set of snapshots would have a good resolution of that phenomenon it is questionable if the 80-dimensional dynamical system could be able represent the dissipation of the eddy in the core.

- From linear stability analysis it follows that the first (Hopf) bifurcation of the 80-dimensional dynamical system takes place at Re=7,819. This is close to value Re=7,972 for the first (Hopf) bifurcation which we found with the DNS. The periods of the periodic solutions are different.
- With the Floquet analysis we found bifurcations in the range Re=8,200-8,750 which we could not find using DNS.
- In the range Re=11,188-11,500 the ratio of the two periods of the 2-periodic solution of the dynamical system is approximately the same as the ratio of the two periods of the 2-periodic solution of the DNS at Re=11,000.
- The periodic solutions of the dynamical system at Re=11,800 and the DNS at Re=12,000 have approximately the same period and have qualitatively the same behavior.